JACS
JOURNAL OF THE AMERICAN CHEMICAL SOCIETY
Article
Cite This: J. Am. Chem. Soc. 2018, 140, 8817−8826
pubs.acs.org/JACS

Pore-Forming Monopeptides as Exceptionally Active Anion Channels

Changliang Ren,[†] Fei Zeng,[†] Jie Shen,[†] Feng Chen,[†] Arundhati Roy,[†] Shaoyuan Zhou,[‡] Haisheng Ren,[‡] and Huaqiang Zeng*[,†]

[†]Institute of Bioengineering and Nanotechnology, 31 Biopolis Way, The Nanos 138669, Singapore
[‡]College of Chemical Engineering, Sichuan University, Chengdu 610065, China

Supporting Information

ABSTRACT: We describe here a unique family of pore-forming anion-transporting peptides possessing a single-amino-acid-derived peptidic backbone that is the shortest among natural and synthetic pore-forming peptides. These monopeptides with built-in H-bonding capacity self-assemble into an H-bonded 1D columnar structure, presenting three types of exteriorly arranged hydrophobic side chains that closely mimic the overall topology of an α-helix. Dynamic interactions among these side chains and membrane lipids proceed in a way likely similar to how α-helix bundle is formed. This subsequently enables oligomerization of these rod-like structures to form ring-shaped ensembles of varying sizes with a pore size of smaller than 1.0 nm in diameter but sufficiently large for transporting anions across the membrane. The intrinsic high modularity in the backbone further allows rapid tuning in side chains for combinatorial optimization of channel's ion-transport activity, culminating in the discovery of an exceptionally active anion-transporting monopeptide **6L10** with an EC_{50} of 0.10 μM for nitrate anions.

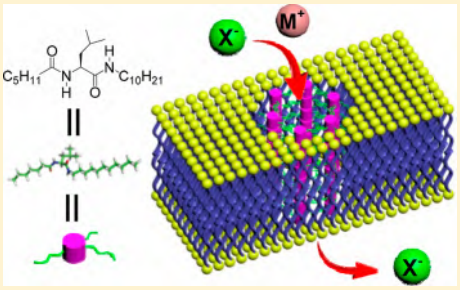

INTRODUCTION

****Naturally occurring pore-forming peptides (PFPs) belong to a large family of host defense peptides.[1,2] They generally share a length of 12−50 amino acids in order to span the hydrophobic membrane region or form a cyclic structure enclosing a sufficiently large cavity, and carry at least one charge in its side chain or termini. With the addition of a long hydrophobic lipid moiety having 12−16 carbon atoms,[3] PFPs can be shortened to as few as 2−4 amino acids.[4,5] Nevertheless, natural[1−4] or synthetic[5−9] PFPs, which are made up of only a single amino acid residue and carry no sophisticated functional group, still remain elusive. We herein report such a unique yet extremely simple class of artificial pore-forming monopeptides to fill this missing gap (Figure 1a).

Our molecular design is inspired by the way α-helices interact with each other to form an α-helix bundle (Figure 1b), a common motif that involves ≥3% of all amino acids in the known genomes for mediating intramolecular protein folding or intermolecular protein−protein interactions.[11] More specifically, two or more α-helices could self-assemble into an α-helix bundle via an interplay of noncovalent forces (van der Waals interactions, $\pi-\pi$ stacking, H-bonds and salt bridges) among the side chains exteriorly arranged around the helical backbone (Figure 1b).[10,12] These α-helix bundles, mostly consisting of 2−8 helices, play a particularly important role in associating multiple subunits to form oligomeric protein complexes of diverse types, including pore-forming toxins[13] and protein channels[14−19] in the cell membrane. They have also proven an excellent target for de novo protein design since 1980s,[20−29] or key components in a range of supramolecular materials.[30−32]

Recently, we showed that amidating both the N- and C-termini of a single amino acid residue using simple groups (Fmoc, Cbz, and alkyl chains, Figure 1a and 1c) gives rise to a rich family of phase-selective organogelators, which are able to rapidly and phase selectively congeal crude oils of widely ranging viscosities in the presence of water at room temperature.[33−35] The crystal structure of **Fmoc-Phe-C4** reveals well-defined one-dimensional packing of the molecules via intermolecular H bonds (Figure 1c).[34] The high directionality of these H bonds packs the same type of side chains (Fmoc, Phe, and C_4H_9) to the same side. A closer examination shows that this H-bonded 1D scaffold with three types of exteriorly arrayed side chains topologically resembles that of an α-helix (Figure 1b vs 1c and 1d), except that the 1D scaffold is noncovalently assembled via H bonds and van der Waals forces while the helically folded backbone in the α-helix is covalent in nature. Hinging on this great similarity in topology and the ability of α-helices to form an α-helix bundle, we hypothesized that monopeptides such as **5L10** might be able to self-assemble into an oligomeric ensemble, likely consisting of 3−8 H-bonded 1D structures, via van der Waals forces among their one-dimensionally aligned side chains (Figure 1d). The intrinsic high modularity involving R_1-R_3 groups should enable rapid screening and optimization of the

Received: May 3, 2018
Published: June 21, 2018

DOI: 10.1021/jacs.8b04657
J. Am. Chem. Soc. 2018, 140, 8817−8826

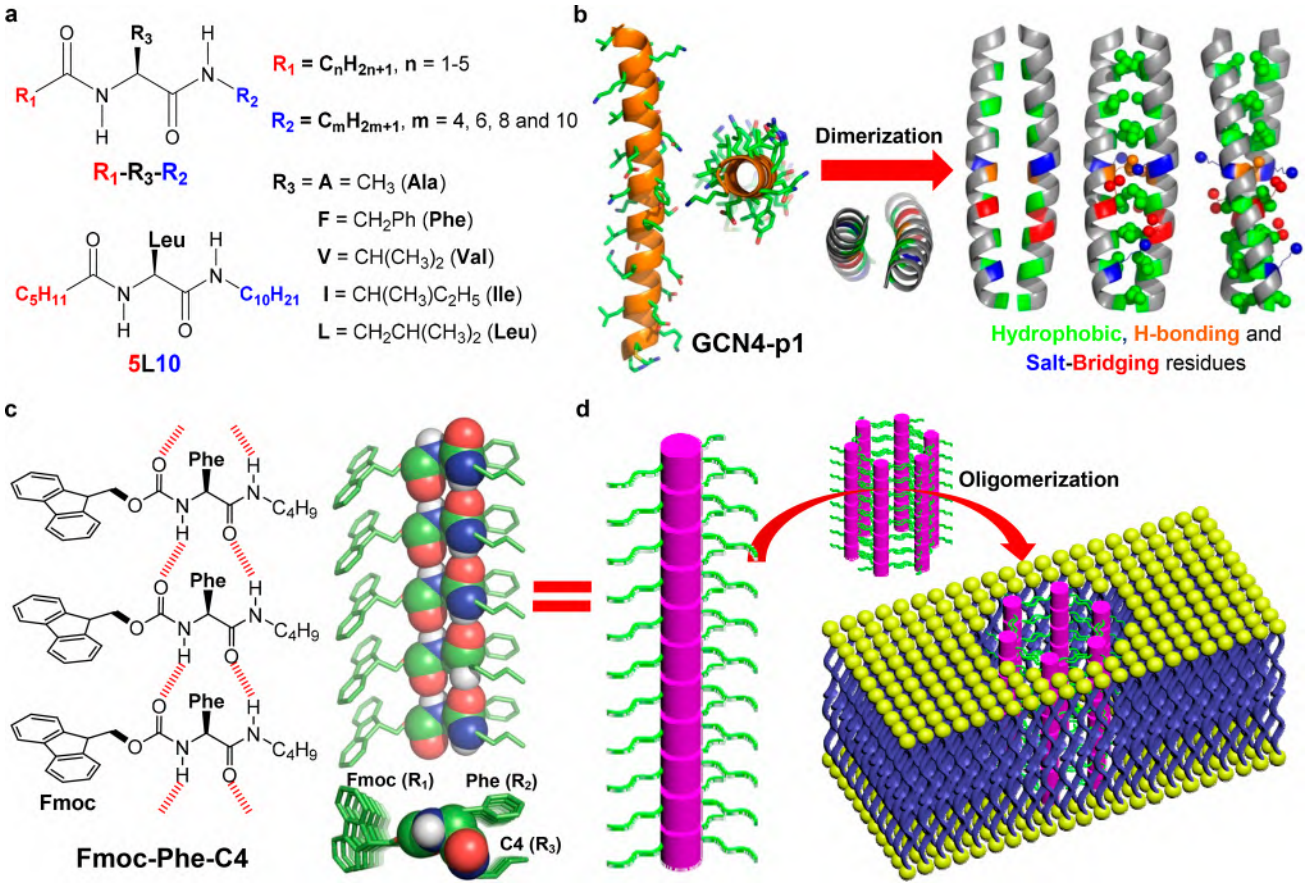

Figure 1. α-Helix-bundle-inspired molecular design of pore-forming monopeptides such as **5L10**. (a) Molecular construction of a pore-forming monopeptide library. (b) Crystal structure of **GCN4-P1**, highlighting various types of noncovalent forces that drive the formation of a two-helix bundle.[10] (c) Crystal structure of **Fmoc-Phe-C4**, illustrating an H-bonded peptidic scaffold with directionally arrayed side chains (e.g., Fmoc, Phe, and C_4H_9). (d) Van der Waals interactions among the one-dimensionally aligned side chains might enable modularly tunable monopeptides (see a) to assemble into such as a hexameric ensemble, possessing a tubular cavity for ion transport. Note that ensembles of other sizes are also possible, and lipid molecules might also participate in the dynamic process of forming such ensembles.

ensemble's properties in the membrane in a combinatorial manner. In a fortunate scenario, the combinatorially identified ensemble(s), alone or through dynamic interplay with membrane lipids, might achieve pore formation that alters the membrane permeability. In this report, we demonstrate that this hypothesis-driven strategy is highly effective, successfully delivering many monopeptides as excellent pore formers with high activity. We further demonstrate that these pore-forming monopeptides conduct anions (chlorides, nitrate, etc.), rather than cations, across the membrane.

RESULTS AND DISCUSSION

Combinatorial Identification of Highly Active Pore Formers. Our first-round combinatorial screening of the ensembles' ion-transport profiles started with 100 monopeptide molecules (5 R_1 × 4 R_2 × 5 R_3, Figure 1a) at a concentration of 5 μM using the pH-sensitive HPTS (8-hydroxypyrene-1,3,6-trisulfonic acid) assay (Figure 2a). In this assay, pH-sensitive HPTS dye (100 μM) and NaCl (100 mM) at pH 7 were encapsulated inside large unilamellar vesicles (LUVs), which were diluted into the same buffer containing no HPTS dye at pH 8 to generate a pH gradient of 7−8 across LUVs. Monitoring pH-dependent changes in the fluorescence intensity of HPTS allows one to compare the channel's capacity in ion transport. From the results summarized in Figure 2b (for ion-transport curves, see Figures S1−S5), two trends, which largely could be correlated to the lipophilicity of molecules, emerge, that is, molecules containing a very short alkyl chain (e.g., C_4H_9) at the R_2 position generally lack good ability to transport ions mostly with a fractional activity (R_{Cl^-}) of <5%, while ion-transport activity apparently increases in increasing order of Val ≈ Ala < Ile < Phe < Leu. In addition, 75, 49, and 26 out of 100 monopeptides display R_{Cl^-} values of ≥5, ≥20%, and ≥50%, respectively. These results suggest a majority of these hypothetic pore-forming peptide molecules indeed could assemble into a defined pore-forming structure of varying stabilities to facilitate ion transport across the membrane, thereby satisfactorily verifying the aforementioned hypothesis.

Monopeptides that more strongly favor pore formation in the membrane were then readily identified by lowering the channel concentration from 5 to 2 μM and further from 2 to 0.4 μM. At 2 μM, 7 molecules (e.g., **5L8**, **5L10**, **4L10**, **3L10**, **5F10**, **4F10**, and **3F10**) could achieve an R_{Cl^-} value of >70% (Figures S6, S10, and S11). Among these molecules, **5L10,** having an R_{Cl^-} value of 65% at 0.4 μM, turns out to be the most active (Figure 2c). On the basis of **5L10**, our secondary screening logically looks into the impact the chain length in both R_1 and R_2 groups might have on ion-transport activity. With R_2 kept constant as $C_{10}H_{21}$, ion-transport studies on ***n*L10** (n = 1−9 and 11) establish **5L10** and **6L10** as the best

DOI: 10.1021/jacs.8b04657
J. Am. Chem. Soc. 2018, 140, 8817−8826

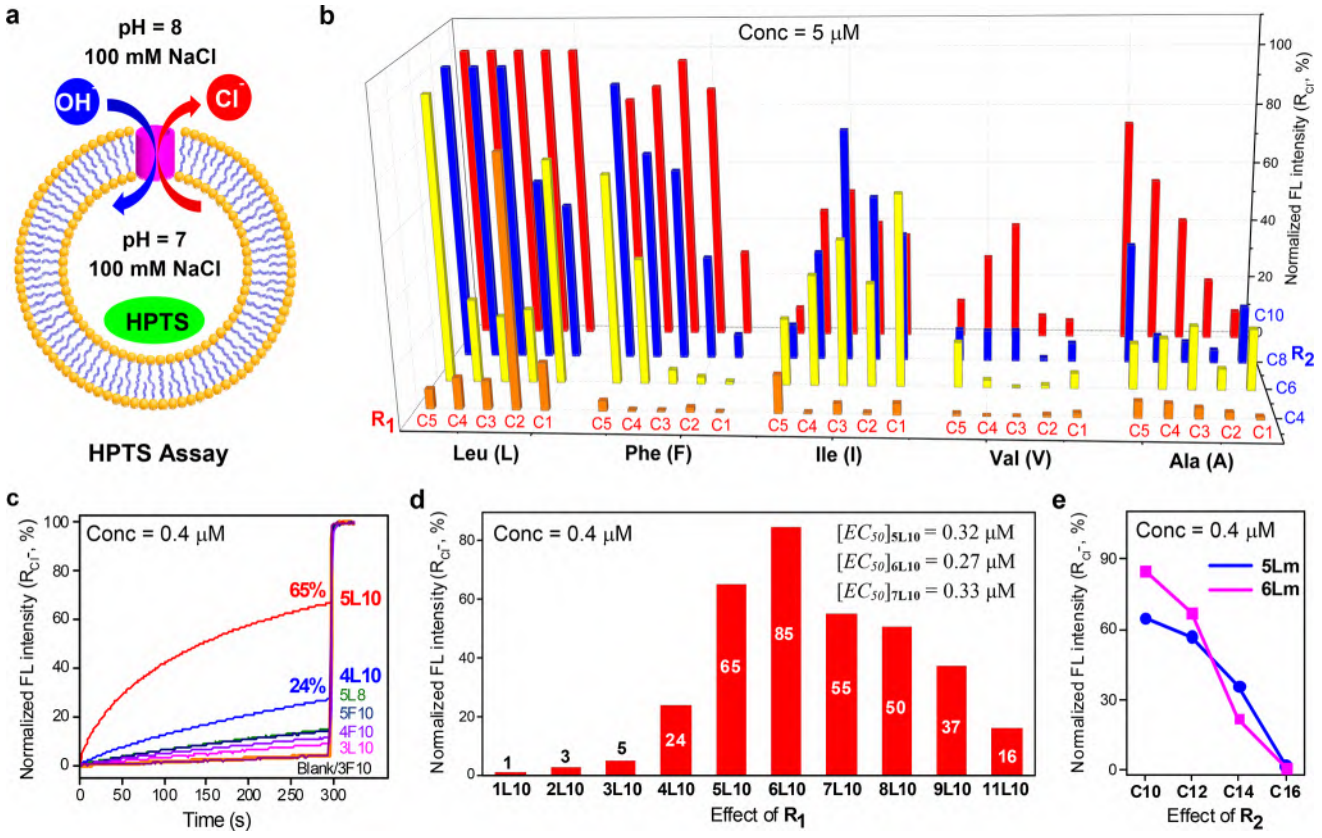

Figure 2. Ion-transport activities of 112 monopeptides determined using the HPTS assay. (a) Schematic illustration of the LUV-based HPTS assay. HPTS refers to 8-hydroxypyrene-1,3,6-trisulfonic acid whose fluorescence intensity increases with increasing pH. (b) Normalized ion-transport activities (R_{Cl^-}) for 100 monopeptides at 5 μM over a duration of 5 min. $R_{Cl^-} = (I_{Cl^-} - I_0)/(I_{Triton} - I_0)$, wherein I_{Cl^-} and I_0 are the ratiometric values of I_{460}/I_{403} before addition of triton at t = 300 s and I_{Triton} is the ratiometric value of I_{460}/I_{403} at t = 300 s right after addition of triton with internal/external buffers containing 100 mM NaCl and a pH gradient of 7−8 across LUVs. Comparative ion-transport activities at 0.4 μM among (c) the seven most active monopeptides from the first-round screening of 100 library members, (d) the ***n*L10** series (n = 1−9 and 11), and (e) the 5L*m* and 6L*m* series (m = 10, 12, 14, and 16).

among the ***n*L10** series (Figures 2d and S12). With R_1 kept constant as C_5H_{11} or C_6H_{13}, continued investigations on two series of channel molecules (**5L*m*** and **6L*m***, m = 10, 12, 14 and 16, Figures 2e and S13) suggest a straight alkyl chain having 10 carbon atoms as the optimum side chain at the R_2 position.

Pore Size and Ion-Transport Activity. Additional experiments using self-quenching CF dye (5(6)-carboxyfluorescein), rather than HPTS dye, trapped inside LUVs show that incorporation of the most active **5L10** and **6L10** at 4 μM into LUVs leads to no leakage of CF dye inside LUVs (Figure S14). For comparison, melittin at 20 nM results in efflux of 71% CF dye from LUVs. From these results it can be inferred that (1) membrane integrity was maintained in the presence of **5L10** and **6L10** at high concentration and (2) the pore formed by **5L10** and **6L10** is smaller than the molecular size of CF dye (1.0 nm, Figure S14).

Using Hill analyses, the EC_{50} values for reaching 50% transmembrane activity were determined to be 0.32 μM for **5L10** and 0.27 μM for **6L10** (Figures 2d and S15a). Previously, the EC_{50} value of the most active giant unimolecular chloride channel, having a molecular weight of 3507 Da and carrying eight linearly arrayed anion-binding units, was determined to be 0.88 μM under identical conditions.[36] On this basis, **6L10**, having a molecular weight of 439 Da, actually is 2.3 times more active than the unimolecular chloride channel. Further, from the crystallographically determined intermolecular distance of 5.0 Å for **Fmoc-Phe-C4** and 4.8 Å for **6L10** (Figure S16), 6−8 peptide molecules are required to span a typical hydrophobic membrane thickness of 28 Å for EYPC-based membrane.[37] Taken together with the fact that only a portion of molecules will undergo self-association to produce an H-bonded 1D columnar structure for facilitated ion transport, the EC_{50} value in terms of effective channel concentration for **6L10** is estimated to be much lower than 0.045 μM (0.27 μM/6). At this concentration, the molar ratio of channel to lipid molecules is as low as 1:711 and comparable to the best natural or synthetic PFPs.[7] This low molar ratio points to a high aptitude of **6L10** in forming a H-bonded 1D structure via H bonds, which subsequently gives rise to a stable pore in the membrane via side chain interactions involving aliphatic side chains from **6L10** and perhaps also lipids.

In addition, we also looked into the effect of cholesterol at up to 30 mol % (relative to EYPC) on the ability of **6L10** to transport chloride anions. At [**6L10**] = 0.45 μM where **6L10** elicits 94% ion-transport activity in the absence of cholesterol, the ion-transport activities decreases to 83%, 80%, 71%, 68%, 64%, and 53% when cholesterol is increasingly present at 5, 10, 15, 20, 25, and 30 mol %, respectively.

OH^-/Cl^- as the Major Transport Species through a Channel Mechanism. Aside from the Cl^-/OH^- antiport mechanism illustrated in Figure 2a, other transport mecha-

DOI: 10.1021/jacs.8b04657
J. Am. Chem. Soc. 2018, 140, 8817−8826

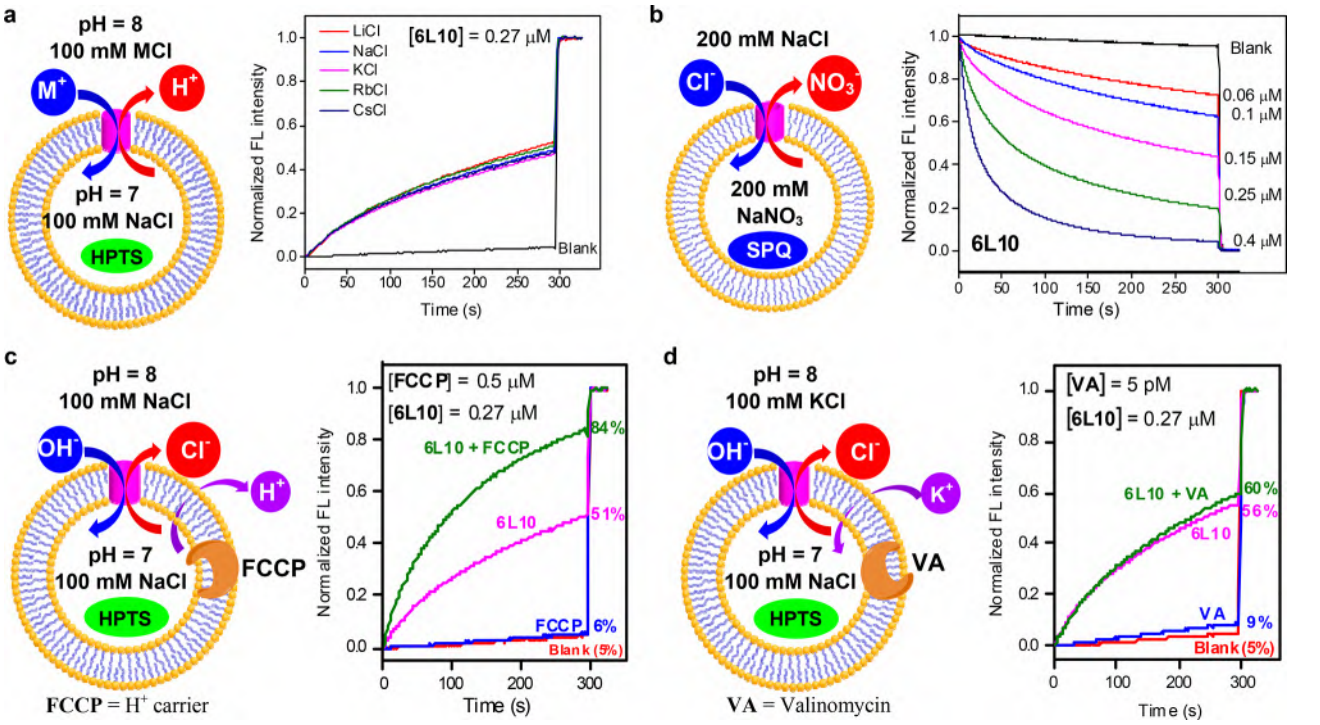

Figure 3. Deciphering ion-transport mechanism and species. (a) HPTS assay using varied extravesicular metal salts (MCl). (b) SPQ assay using a chloride-sensitive SPQ dye. (c) HPTS assay using a proton carrier FCCP. (d) HPTS assay using a potassium carrier valinomycin.

nisms and species, including Na^+/H^+ antiport, Na^+/OH^- symport, and Cl^-/H^+ symport, might also be responsible for the observed increase in pH inside LUVs, leading to a time-dependent enhancement in fluorescence intensity of HPTS. To elucidate the most likely transport mechanism and species, a range of experiments was carried out on **6L10**. First, extravesicular metal chloride salts were varied from LiCl to CsCl, and insignificant changes in the fluorescence intensity of HPTS upon these variations is indicative of little involvement of metal ions in the **6L10**-mediated ion-transport process (Figure 3a). Second, increasing additions of **6L10** from 0.06 to 0.4 μM cause concentration-dependent increasing quenching of fluorescence of a chloride-sensitive SPQ dye ((6-methoxy-*N*-(3-sulfopropyl) quinolinium)), revealing chloride anion as one of the true transport species (Figure 3b). These two lines of evidence allow us to confidently conclude that rather than the M^+/H^+ antiport or M^+/OH^- symport, either the OH^-/Cl^- antiport (Figure 2a) or the H^+/Cl^- symport mechanism is the predominant mechanism operational in **6L10**-mediated ion transport.

A highly active proton carrier, FCCP (carbonyl cyanide 4-(trifluoromethoxy)phenylhydrazone), was employed to differentiate the two possible mechanisms (Figure 3c). Relative to the transport efficiencies of 6% for FCCP alone and of 51% for **6L10** alone, a large enhancement of 22% in transport efficiency (e.g., 84% − 51% − (6% − 5%) by **6L10** in the presence of FCCP indicates a strong cooperative action between **6L10** and FCCP and that Cl^- is transported faster than H^+.[38]

As for the relative transport rate between OH^- and Cl^-, we also performed the HPTS assay in the presence of valinomycin (VA), a K^+-selective carrier (Figure 3d). We found that the ion-transport activities of **6L10** (0.27 μM) in the presence and absence of of valinomycin (5 pM) differs very slightly by 4%, a difference that is identical to that between VA (9%) and blank (5%). These results not only suggest Cl^- to be transported faster than OH^- but also are consistent with a negligible role played by the H^+/M^+ antiport mechanism.[38]

Using a Planar Lipid Bilayer Workstation (Warner Instruments), the ion-conducting behavior of **6L10** was assessed in symmetric baths (cis chamber = trans chamber = 1 M KCl, Figure 4a). The evolved single-channel current trace unequivocally confirms that **6L10**-mediated chloride transport proceeds through a channel, rather than a carrier mechanism. Since the vertically aligned amide groups in the H-bonded 1D chain made up of eight **6L10** molecules apparently are not readily accessible for binding and mediating transport of a hydrated chloride anion (Figures 5a and S16a), we therefore

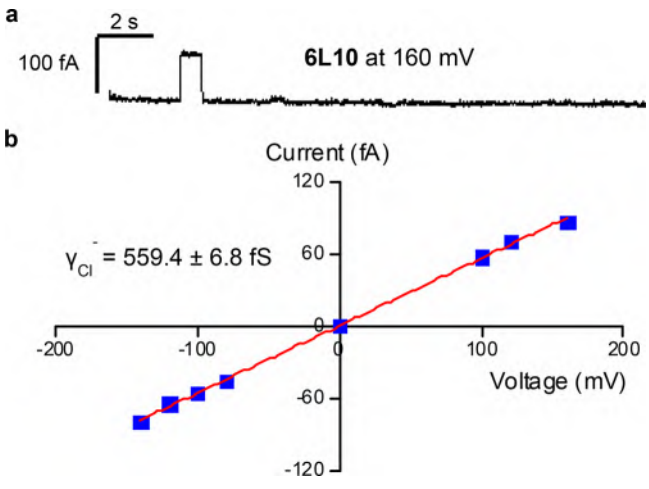

Figure 4. Single-channel current measurement in planar lipid bilayers and determination of anion selectivity. (a) Single-channel current trace recorded in symmetric baths (cis chamber = trans chamber = 1 M KCl) at 160 mv for **6L10**. (b) Determination of Cl^- conductance (γ_{Cl}^-) for **6L10** using a linear ohmic current−voltage (*I*−*V*).

DOI: 10.1021/jacs.8b04657
J. Am. Chem. Soc. 2018, 140, 8817−8826

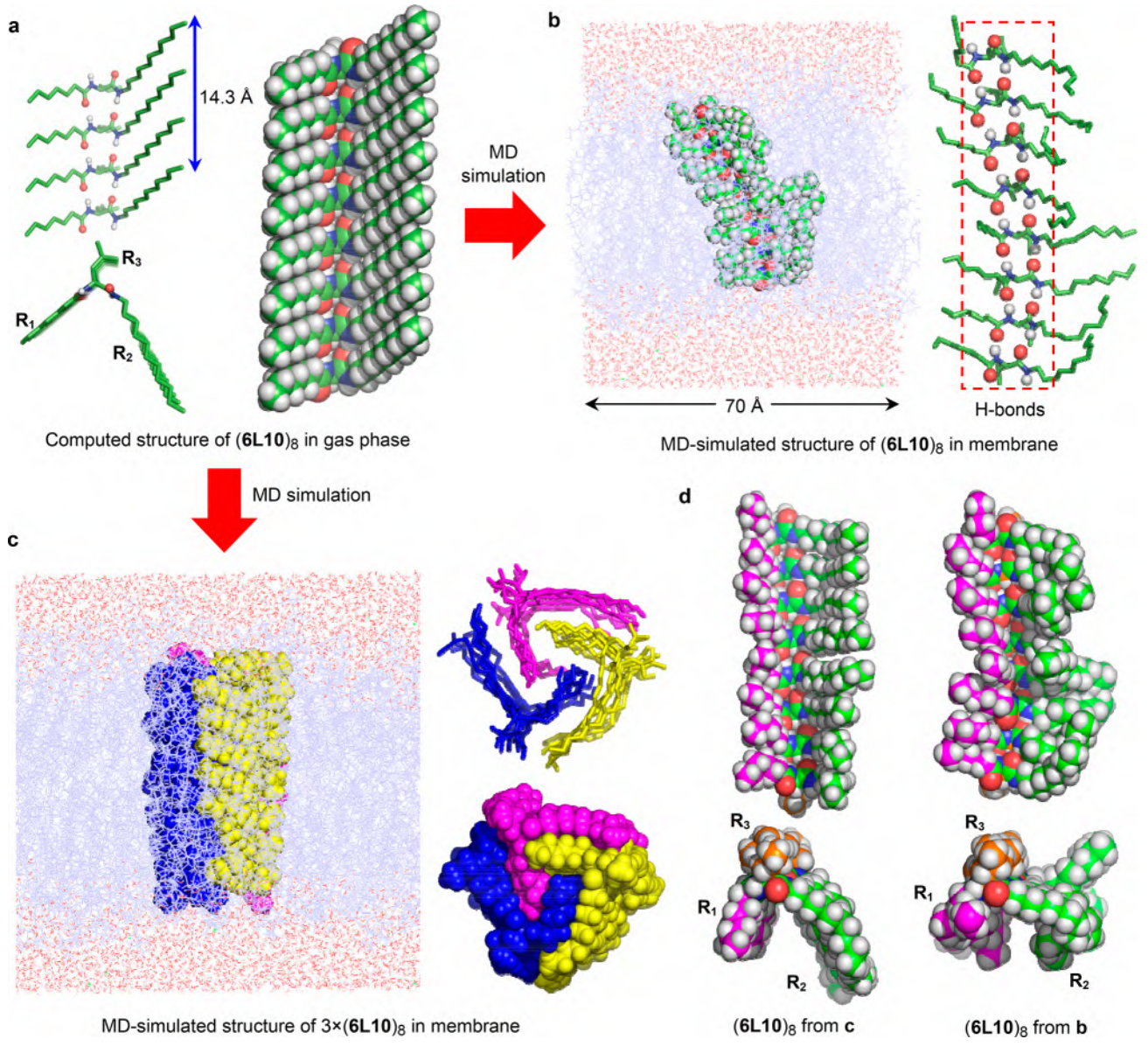

Figure 5. Computationally optimized structures for H-bonded $(\mathbf{6L10})_8$ in the gas phase and in lipid membrane. (a) Computed structure of $(\mathbf{6L10})_8$ using the COMPASS force field.[45] (b) MD-simulated structure of $(\mathbf{6L10})_8$ inside a simulation box of 70 Å (w) × 70 Å (w) × 74 Å (h), comprising 128 POPC molecules and 4794 water molecules. (c) MD-simulated structure of 3 × $(\mathbf{6L10})_8$ in DOPC membrane. (d) Structural comparison between MD-simulated structures of $(\mathbf{6L10})_8$ from b and c. POPC = 1-palmitoyl-2-oleoyl-*sn*-glycero-3-phosphocholine.

proposed a barrel-stave pore model for chloride transport (Figure 1d). In this model, 3−8 H-bonded 1D chains self-assemble into an oligomeric pore such as a hexameric pore of <1.0 nm in diameter through interactions among alkyl chains at the R_1−R_3 positions. It is highly likely that these pore-forming peptides and lipid molecules might also cooperate and remodel each other to achieve formation of a pore with optimum performance. In either scenario it is anticipated that the pore formed this way is mostly lined up by hydrophobic alkyl chains. In view of opposite orientations of water molecules in the hydration shell of cations and anions, these alkyl chains, which line the pore and carry many slightly positively charged H atoms, undoubtedly will interact more favorably, albeit weakly, with O atoms from water molecules in the hydration shell of anions than with hydrated cations including protons. This reasoning is in good accord with our experimental finding on preferential transport of chloride over sodium ions or protons (Figure 3a) and with the fact that many other H-bonded monopeptide-based molecules show low or extremely low activity (Figure 1b), thereby suggesting an unlikelihood of having Cl^-/H^+ cotransport as the major transport species. Using single-channel current traces recorded at various voltages, a linear ohmic current−voltage (I−V) curve could be generated from which the Cl^- conductance (γ_{Cl}^-) for **6L10** was determined to be 559.4 ± 6.8 fS (Figures 4b and S17).

The above set of experiments performed on **6L10** was also carried out on **5L10**. Similar to **6L10**, experimental findings on **5L10** are also supportive of (1) OH^-/Cl^- antiport as the main transport mechanism and species (Figure S18), (2) anion transport occurring through a channel mechanism with Cl^- conductance of 552.8 ± 5.5 fS (Figure S19), and (3) high activity (EC_{50} = 0.32 μM, Figure S15a).

DOI: 10.1021/jacs.8b04657
J. Am. Chem. Soc. 2018, 140, 8817−8826

We further determined the EC_{50} values for the next best five pore formers (e.g., **4L10**, **7L10**, **8L10**, **5L12**, and **6L12**) as well as the best transporter from each of the other four amino acid series (e.g., **5A10** for alanine, **3V10** for valine, **3I8** for isoleucine, and **5F10** for phenylalanine). As summarized in Table 1 and Figure S15, having EC_{50} values of 0.27−0.53 μM,

Table 1. EC_{50} Values for *n*L10 (*n* = 4−8), *m*L12 (*m* = 5, 6), 5A10, 3V10, 3I8, and 5F10 Determined Using the HPTS Assay

	4L10	5L10	6L10	7L10	8L10	5L12
EC_{50} (μM)	0.53	0.32	0.27	0.33	0.39	0.36
n value[a]	4.7	3.3	3.5	3.4	3.1	3.8
	6L12	**5A10**	**3V10**	**3I8**	**5F10**	
EC_{50} (μM)	0.32	4.0	7.6	2.5	0.73	
n value[a]	3.5	3.8	1.3	1.5	3.5	

[a]Hill cofficient.

the seven leucine derivatives are the most active among all 112 monopeptides tested in this work and much better than the best four pore-formers derived from the other four types of amino acids (**A**, **V**, **I**, and **F**). The Hill coefficient values of 1.3−3.7 for these 11 channels (Table 1) are consistent with the fact that the functional channels are self-assembled from multiple molecules.

Anion Selectivity. The best two pore formers **5L10** and **6L10** were chosen for further comparing their selectivity in anion transport toward five types of anions (e.g., Cl^-, Br^-, I^-, NO_3^-, and ClO_4^-). In these LUV-based experiments for determining anion selectivity, the same type and identical concentration of sodium salts (NaX at 100 mM) were used in both intra- and extravesicular regions with a proton gradient from pH 7 (inside) to pH 8 (outside). Comparison of EC_{50} values determined for five anions using Hill plots reveals the same selectivity trend, i.e., $Cl^- < I^- < Br^- < ClO_4^- < NO_3^-$, for **5L10** and **6L10** with the nitrate anions as the most preferred transport species (Figures 6, S20, and S21). In more detail, the EC_{50} values are 0.32, 0.30, 0.24, 0.20, and 0.15 μM for Cl^-, I^-, Br^-, ClO_4^-, and NO_3^- for **5L10**, respectively. For **6L10**, these

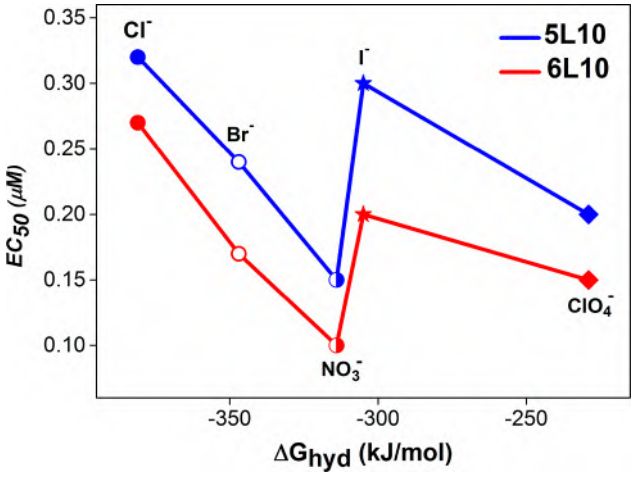

Figure 6. EC_{50} values vs hydration energies for **5L10**- and **6L10**-mediated transport of Cl^-, Br^-, I^-, NO_3^-, and ClO_4^- determined using the HPTS assay with both intra- and extravesicular regions containing the same type of NaX at 100 mM and a pH gradient of 7−8 across LUVs.

values are 0.27, 0.20, 0.17, 0.15, and 0.10 μM, respectively. As expected, **6L10** performs better than **5L10** in transporting all five types of anions. In the same way as analyzed above for chloride transport, the effective channel concentration for **6L10** to transport NO_3^- anions is much lower than 0.017 μM (0.10 μM/6), which corresponds to an extremely low channel:lipid molar ratio of 1:1920.

Conformation and Stability of H-Bonded Structure in POPC Membrane. The dynamic interactions between pore-forming peptides/proteins and lipids often play a decisive role in the pore-forming process.[8,39−43] For instance, the majority of pore-forming peptides are unstructured in solution and form functional pores only upon membrane binding/insertion.[8,39,40] Even more interestingly, depending on lipid compositions, complete or partially formed pores are possible for pore-forming proteins such as membrane attack complex−perforin.[41−43] In our current study, although the experimental evidence obtained using the HPTS assay and single-channel current measurement unambiguously confirm the formation of well-defined channels for facilitated transport of anions across lipid membrane, it has remained quite challenging both experimentally and computationally to elucidate the pore structures or how the pores are formed. Nevertheless, it is feasible to at least shed some light into possible structural features of the one-dimensionally aligned structure involving **6L10** in lipid membrane. In this regard, we first applied the COMPASS force field[44] to optimize the H-bonded 1D structure, which consists of eight molecules of **6L10**, and then embedded the optimized 1D structure in a bilayer of 128 POPC molecules (17 152 atoms) solvated on two sides by 2 × 2397 water molecules, leading to a simulation system of 32 062 atoms with dimensions of 70 Å (w) × 70 Å (w) × 74 Å (h) (Figure 5). Molecular dynamics (MD) simulation using the CHARMM program,[45−49] PME method,[50] and SHAKE algorithm[51] was then carried out on this simulation system. After equilibration steps, the production run was carried out for 25 ns. The last 10 ns trajectories with 500 structural snapshots were used for analyzing conformations of H-bonded structure in lipid membrane. Examining these 500 structures shows that (1) all side chains at the R_1, R_2, and R_3 positions, which are superimposable over each other in the initial structure (Figure 5a), become much less organized as evidenced from the highly populated structure shown in Figure 5b and 5d and (2) all eight molecules of **6L10** persistently remain H bonded to each other in all 500 structures surveyed, demonstrating the reliability of intermolecular H bonds in forming a H-bonded 1D structure able to span the hydrophobic membrane region.

As shown in Figure S16a, **6L10** can have another energetically equivalent conformation where the angle formed by R_1 and R_2 groups is about 145°. For this alternative structure, MD simulation converges on the same conclusions (Figure S16b).

Further simulation on a trimeric ensemble comprising three H-bonded $(\mathbf{6L10})_8$ in membrane supports the notion, as illustrated in Figure 1d, that intermolecular association among the projected side chains in H-bonded assembly $(\mathbf{6L10})_8$ indeed could exist in lipid membrane (Figure 5c). Structural comparison compiled in Figure 5d indicates that a positive feedback mechanism might be operational during the self-assembly process, that is, interchain association helps to better organize side chains in a way to increase the self-association extent. However, given that (1) **6L10** has two energetically

DOI: 10.1021/jacs.8b04657
J. Am. Chem. Soc. 2018, 140, 8817−8826

equivalent conformations (Figures 5a and S16a) and (2) lipid molecules may also participate to modulate the assembled structures, we do anticipate the channel-forming process to be very complex, which certainly is beyond the scope of the present work.

CONCLUSION

To summarize, in analogy to the way widely known α-helix bundles are formed from α-helices, we successfully designed and demonstrated a novel class of pore-forming monopeptides. These pore formers are very unusual and unprecedented in that their backbone consists of only a single amino acid residue, amidated at two termini with simple alkyl chains to assist formation of a H-bonded 1D columnar structure. These 1D structures resemble the topology of α-helices and associate to generate pore-forming oligomeric ensembles conducible for highly efficient anion transport. The best of them exhibits exceptionally high anion-transport activity when compared to other artificial anion channels elaborated over the past years.[36,38,52−65] In particular, the EC_{50} value for **6L10**-mediated transport of nitrate anions reaches as low as 0.10 or 0.017 μM (0.05 mol % relative to lipid) in terms of effective channel concentration.

EXPERIMENTAL SECTION

Proton Transport Study Using the HPTS Assay and EC_{50} Measurements Using the Hill Analysis. Egg yolk L-α-phosphatidylcholine (EYPC, 1 mL, 25 mg/mL in $CHCl_3$, Avanti Polar Lipids, USA) and MeOH (1 mL) were mixed in a round-bottom flask. The mixed solvents were removed under reduced pressure at 40 °C. After drying the resulting film under high vacuum overnight at room temperature, the film was hydrated with 4-(2-hydroxyethyl)-1-piperazine-ethanesulfonic acid (HEPES) buffer solution (1 mL, 10 mM HEPES, 100 mM NaCl, pH = 7.0) containing a pH-sensitive dye 8-hydroxypyrene-1,3,6-trisulfonic acid (HPTS, 1 mM) at room temperature for 60 min to give a milky suspension. The mixture was then subjected to 12 freeze−thaw cycles: freezing in liquid N_2 for 1 min and heating 37 °C water bath for 1.5 min. The vesicle suspension was extruded through polycarbonate membrane (0.1 μm) to produce a homogeneous suspension of large unilamellar vesicles (LUVs) of about 120 nm in diameter with HPTS encapsulated inside. The unencapsulated HPTS dye was separated from the LUVs by using size exclusion chromatography (stationary phase Sephadex G-50, GE Healthcare, USA; mobile phase HEPES buffer with 100 Mm NaCl) and diluted with the mobile phase to yield 12.8 mL of 2.5 mM lipid stock solution. The HPTS-containing LUV suspension (25 μL, 2.5 mM in 10 mM HEPES buffer containing 100 mM NaCl at pH = 7.0) was added to a HEPES buffer solution (1.93 mL, 10 mM HEPES, 100 mM NaCl at pH = 8.0) to create a pH gradient for ion-transport study. A solution of channel molecules in DMSO was then injected into the suspension under gentle stirring. Upon addition of channels, the emission of HPTS was immediately monitored at 510 nm with excitations at both 460 and 403 nm recorded simultaneously for 300 s using a fluorescence spectrophotometer (Hitachi, model F-7100, Japan) after which time an aqueous solution of Triton X-100 (20 μL, 20% v/v) was immediately added to achieve the maximum change in dye fluorescence emission. The final transport trace was obtained after subtracting background intensity at t = 0, as a ratiometric value of I_{460}/I_{403} and normalized based on the ratiometric value of I_{460}/I_{403} after addition of triton. The fractional changes R_{Cl^-} was calculated for each curve using the normalized value of I_{460}/I_{403} at 300 s before addition of triton, with triton with a ratiometric value of I_{460}/I_{403} at t = 0 s as 0% and that of I_{460}/I_{403} at t = 300 s (obtained after addition of triton) as 100%. Fitting the fractional transmembrane activity R_{Cl^-} vs channel concentration using the Hill equation $Y = 1/(1+ (EC_{50}/[C])^n)$ gave the Hill coefficient n and EC_{50} values.

HPTS Assay for Cation Selectivity. The HPTS-containing LUV suspension (25 μL, 2.5 mM in 10 mM HEPES buffer containing 100 mM NaCl at pH = 7.0) was added to a HEPES buffer solution (1.93 mL, 10 mM HEPES, 100 mM MCl at pH = 8.0, where M^+= Li^+, Na^+, K^+, Rb^+, and Cs^+) to create a pH gradient for ion-transport study. A solution of monopeptide molecules **5L10** or **6L10** at a final concentration of 0.32 or 0.27 μM (EC_{50}) in DMSO was then injected into the suspension under gentle stirring. Upon addition of channels, the emission of HPTS was immediately monitored at 510 nm with excitations at both 460 and 403 nm recorded simultaneously for 300 s using a fluorescence spectrophotometer (Hitachi, model F-7100, Japan) after which time an aqueous solution of Triton X-100 (20 μL, 20% v/v) was immediately added to achieve the maximum change in dye fluorescence emission. The final transport trace was obtained as a ratiometric value of I_{460}/I_{403} and normalized based on the ratiometric value of I_{460}/I_{403} after addition of triton.

HPTS Assay for Anion Selectivity. The HPTS-containing LUV suspension (25 μL, 2.5 mM in 10 mM HEPES buffer containing 100 mM NaX where X^- = Cl^-, Br^-, I^-, NO_3^-, and ClO_4^- at pH = 7.0) was added to a HEPES buffer solution (1.93 mL, 10 mM HEPES, 100 mM NaX, where X^-= Cl^-, Br^-, I^-, NO_3^-, and ClO_4^- at pH = 8.0) to create a pH gradient for ion-transport study. A solution of **5L10** or **6L10** at a final concentration of 0.32 or 0.27 μM (EC_{50}) in DMSO was then injected into the suspension under gentle stirring. Upon addition of pore-forming monopeptide molecules, the emission of HPTS was immediately monitored at 510 nm with excitations at both 460 and 403 nm recorded simultaneously for 300 s using a fluorescence spectrophotometer (Hitachi, model F-7100, Japan) after which time an aqueous solution of Triton X-100 (20 μL, 20% v/v) was immediately added to achieve the maximum change in dye fluorescence emission. The final transport trace was obtained as a ratiometric value of I_{460}/I_{403} and normalized based on the ratiometric value of I_{460}/I_{403} after addition of triton.

HPTS Assay in the Presence of FCCP (carbonyl cyanide-4-(trifluoromethoxy)phenylhydrazone). The HPTS-containing LUV suspension (25 μL, 2.5 mM in 10 mM HEPES buffer containing 100 mM NaCl at pH = 7.0) was added to a HEPES buffer solution (1.93 mL, 10 mM HEPES, 100 mM NaCl) to create a pH gradient for ion-transport study. A solution of FCCP (0.5 μM) and **5L10** (0.32 μM) or **6L10** (0.27 μM) in DMSO was then injected into the suspension under gentle stirring at 20 and 70 s, respectively. Upon addition of pore-forming monopeptide molecules, the emission of HPTS was immediately monitored at 510 nm with excitations at both 460 and 403 nm recorded simultaneously for 300 s using a fluorescence spectrophotometer (Hitachi, model F-7100, Japan). Three hundred second later, an aqueous solution of Triton X-100 (20 μL, 20% v/v) was immediately added to achieve the maximum change in dye fluorescence emission. The final transport trace was obtained as a ratiometric value of I_{460}/I_{403} and normalized based on the ratiometric value of I_{460}/I_{403} after addition of triton.

HPTS Assay in the Presence of Valinomycin (VA). The HPTS-containing LUV suspension (25 μL, 2.5 mM in 10 mM HEPES buffer containing 100 mM NaCl at pH = 7.0) was added to a HEPES buffer solution (1.93 mL, 10 mM HEPES, 100 mM NaCl) to create a pH gradient for ion-transport study. A solution of valinomycin (5 pM) and **5L10** (0.32 μM) or **6L10** (0.27 μM) in DMSO was then injected into the suspension under gentle stirring for 20 and 70 s, respectively. Upon addition of pore-forming monopeptide molecules, the emission of HPTS was immediately monitored at 510 nm with excitations at both 460 and 403 nm recorded simultaneously for 300 s using a fluorescence spectrophotometer (Hitachi, model F-7100, Japan) after which time an aqueous solution of Triton X-100 (20 μL, 20% v/v) was immediately added to achieve the maximum change in dye fluorescence emission. The final transport trace was obtained as a ratiometric value of I_{460}/I_{403} and normalized based on the ratiometric value of I_{460}/I_{403} after addition of triton.

Membrane Leaking and Pore Size Determination Using CF Dye. Egg yolk L-α-phosphatidylcholine (EYPC, 1 mL, 25 mg/mL in $CHCl_3$, Avanti Polar Lipids, USA) and MeOH (1 mL) were mixed in a round-bottom flask. The mixed solvents were removed under

DOI: 10.1021/jacs.8b04657
J. Am. Chem. Soc. 2018, 140, 8817−8826

reduced pressure at 40 °C. After drying the resulting film under high vacuum overnight at room temperature, the film was hydrated with HEPES buffer solution (1 mL, 10 mM HEPES, 100 mM NaCl, pH = 7.5) containing a 5(6)-fluorescein (CF, 50 mM) at room temperature for 60 min to give a milky suspension. The mixture was then subjected to 12 freeze−thaw cycles: freezing in liquid N_2 for 1 min and heating at 37 °C in water bath for 1.5 min. The vesicle suspension was extruded through polycarbonate membrane (0.1 μm) to produce a homogeneous suspension of large unilamellar vesicles (LUVs) of about 120 nm in diameter with CF encapsulated inside. The free unencapsulated CF dye was separated from the LUVs by using size exclusion chromatography (stationary phase Sephadex G-50, GE Healthcare, USA; mobile phase HEPES buffer with 100 mM NaCl) and diluted with the mobile phase to yield 12.8 mL of 2.5 mM lipid stock solution.

The CF-containing LUV suspension (25 μL, 2.5 mM in 10 mM HEPES buffer containing 100 mM NaCl at pH = 7.5) was added to a HEPES buffer solution (1.93 mL, 10 mM HEPES, 100 mM NaCl at pH = 7.5) to create a concentration gradient for CF dye transport study. A solution of **5L10** or **6L10** (4 μM) or natural pore-forming peptide Melittin in DMSO at different concentrations was then injected into the suspension under gentle stirring. Upon addition of pore-forming monopeptide molecules, the emission of CF was immediately monitored at 517 nm with excitations at 492 nm for 300 s using a fluorescence spectrophotometer (Hitachi, model F-7100, Japan), after which time an aqueous solution of Triton X-100 (20 μL, 20% v/v) was immediately added to completely destruct the chloride gradient. The final transport trace was obtained by normalizing the fluorescence intensity using the equation of $I_f = [(I_t - I_0)/(I_1 - I_0)]$, where I_f = fractional emission intensity, I_t = fluorescence intensity at time t, I_1 = fluorescence intensity after addition of Triton X-100, and I_0 = initial fluorescence intensity.

Chloride Transport Using the SPQ Assay. Egg yolk L-α-phosphatidylcholine (EYPC, 1 mL, 25 mg/mL in $CHCl_3$, Avanti Polar Lipids, USA) and MeOH (1 mL) were mixed in a round-bottom flask. The mixed solvents were removed under reduced pressure at 40 °C. After drying the resulting film under high vacuum overnight at room temperature, the film was hydrated with $NaNO_3$ solution (1 mL, 200 mM) containing a Cl^--sensitive dye 6-methoxy-*N*-(3-sulfopropyl)quinolinium (SPQ) (0.5 mM) in a thermostatic shaker−incubator at room temperature for 60 min to give a milky suspension. The mixture was then subjected to 12 freeze−thaw cycles: freezing in liquid N_2 for 1 min and heating at 37 °C in water bath for 1.5 min. The vesicle suspension was extruded through polycarbonate membrane (0.1 μm) to produce a homogeneous suspension of large unilamellar vesicles (LUVs) of about 120 nm in diameter with SPQ encapsulated inside. The unencapsulated HPTS dye was separated from the LUVs by using size exclusion chromatography (stationary phase Sephadex G-50, GE Healthcare, USA; mobile phase 200 mM $NaNO_3$) and diluted with the mobile phase to yield 12.8 mL of 2.5 mM lipid stock solution.

The SPQ-containing LUV suspension (25 μL, 2.5 mM in 200 mM $NaNO_3$) was added to a NaCl solution (1.93 mL, 200 mM) to create an extravesicular chloride gradient. A solution of monopeptide molecule **5L10** or **6L10** in DMSO at different concentrations was then injected into the suspension under gentle stirring. Upon addition of pore-forming monopeptide molecules, the emission of SPQ was immediately monitored at 430 nm with excitations at 360 nm for 300 s using a fluorescence spectrophotometer (Hitachi, model F-7100, Japan) after which time an aqueous solution of Triton X-100 (20 μL, 20% v/v) was immediately added to completely destruct the chloride gradient. The final transport trace was obtained by normalizing the fluorescence intensity using the equation $I_f = [(I_t - I_1)/(I_0 - I_1)]$, where I_f = fractional emission intensity, I_t = fluorescence intensity at time t, I_1 = fluorescence intensity after addition of Triton X-100, and I_0 = initial fluorescence intensity.

Single-Channel Current Measurement in Planar Lipid Bilayers. The chloroform solution of 1,2-diphytanoyl-*sn*-glycero-3-phosphocholine (diPhyPC, 10 mg/mL, 20 uL) was evaporated using nitrogen gas to form a thin film and redissolved in *n*-decane (8 μL). A 0.2 μL amount of this *n*-decane solution was injected into the aperture (diameter = 200 um) of the Delrin cup (Warner Instruments, Hamden, CT) with the *n*-decane removed using nitrogen gas. In a typical experiment for conductance measurement, both the chamber (cis side) and the Delrin cup (trans side) were filled with an aqueous KCl solution (1.0 M, 1.0 mL). Ag−AgCl electrodes were inserted into the two solutions with the cis chamber grounded. Planar lipid bilayer was formed by painting 0.3 μL of the lipid-containing *n*-decane solution around the *n*-decane-pretreated aperture. Successful formation of planar lipid bilayers can be established with a capacitance value ranging from 80 to 120 pF. Samples (**5L10** or **6L10**) in THF (0.3−1.0 μL) were added to the cis compartment to reach a final concentration of around 10^{-8} M, and the solution was stirred for a few minutes until a single current trace appeared. These single-channel currents were then measured using a Warner BC-535D bilayer clamp amplifier, collected by PatchMaster (HEKA) with a sample interval at 5 kHz, and filtered with an 8-pole Bessel filter at 1 kHz (HEKA). The data were analyzed by FitMaster (HEKA) with a digital filter at 100 Hz. Plotting current trace vs voltage yielded chloride conductance (γ_{Cl-}).

Molecular Modeling Using the COMPASS Force Field. The COMPASS force field (condensed-phase optimized molecular potentials for atomistic simulation studies) developed by Sun[44] was used to optimize the geometry and to calculate the energy of all molecules. The COMPASS force field is based on state-of-the-art ab initio and empirical parametrization techniques with the valence parameters and atomic partial charges supported by ab initio data and the van der Waals (vdW) parameters derived by fitting the experimental data of cohesive energies and equilibrium densities. The convergence tolerance is 2×10^{-5} kcal/mol for the energy, 0.001 kcal/mol/Å for the force, 0.001 GPa for the stress, and 10^{-5} Å for the displacement. The Ewald method is used for calculating the electrostatic and van der Waals terms. The accuracy is 10^{-5} kcal/mol. The repulsive cutoff is 6 Å for the van der Waals term. For the periodical structure, the box vector along the stacking direction is also optimized together with the molecules.

Molecular Dynamics Simulations. Membrane builder in CHARM-GUI[45,46] is used to build the initial structure. The protocol comprises six steps as described by Jo et al.,[47] which are sequentially performed in the following order: objects reading, objects orientation, system size determination, building of lipid bilayer, assembly of lipid bilayer, and system equilibrium. In this work, the H-bonded structure, consisting of eight molecules of **L8** (528 atoms), is placed in the center of the membrane made up of 128 molecules of 1-palmitoyl-2-oleoyl-*sn*-glycero- 3-phosphocholine (POPC) and a total of 17 152 atoms. The membrane is then placed in a box of 70 Å × 70 Å in width and 74 Å in height. There were 4794 water molecules placed on the top side and bottom side of the membrane (2397 each side). Counter KCl ions were added to produce an ion concentration of 0.15 M. The simulation used the CHARMM36 (C36) force field[48] for lipids, CHARMM General Force Field (CGenFF)[48] for the repeating unit of L8, and the CHARMM TIP3P water model.[49] The periodic boundary condition (PBC) was employed, and the particle mesh Ewald (PME) method[50] was used for long-range electrostatic interactions. The simulation time step was set to 2 fs in conjunction with the SHAKE algorithm[51] to constrain the covalent bonds involving hydrogen atoms. The constructed system is first relaxed through molecular mechanics (MM) minimization of 20 000 steps, then heated to 303.15 K using 50 ps NPT molecular dynamics (MD) simulations, and finally equilibrated using 200 ps NPT MD simulations. During MD simulations, the pressure was maintained at 1 bar. After equilibration steps, the production run of simulation was performed for 25 ns and the last 10 ns trajectories with 500 structures were used for analyzing the conformation and stability of the H-boned structure.

■ ASSOCIATED CONTENT

Supporting Information

The Supporting Information is available free of charge on the ACS Publications website at DOI: 10.1021/jacs.8b04657.

DOI: 10.1021/jacs.8b04657
J. Am. Chem. Soc. 2018, 140, 8817−8826

Synthetic procedures for 112 monopeptides as well as a full set of characterization data including ^{1}H NMR, ^{13}C NMR, MS, ion-transport study, CF assay, single-channel current experiment, and computational details (PDF)

AUTHOR INFORMATION

Corresponding Author

*hqzeng@ibn.a-star.edu.sg

ORCID

Huaqiang Zeng: 0000-0002-8246-2000

Notes

The authors declare no competing financial interest.

ACKNOWLEDGMENTS

This work was supported by the Institute of Bioengineering and Nanotechnology (Biomedical Research Council, Agency for Science, Technology and Research, Singapore).

REFERENCES

(1) Lai, Y.; Gallo, R. L. *Trends Immunol.* **2009**, *30*, 131.
(2) Hancock, R. E. W.; Haney, E. F.; Gill, E. E. *Nat. Rev. Immunol.* **2016**, *16*, 321.
(3) Mandal, S. M.; Sharma, S.; Pinnaka, A. K.; Kumari, A.; Korpole, S. *BMC Microbiol.* **2013**, *13*, 152.
(4) Tareq, F. S.; Lee, M. A.; Lee, H.-S.; Lee, Y.-J.; Lee, J. S.; Hasan, C. M.; Islam, M. T.; Shin, H. J. *Org. Lett.* **2014**, *16*, 928.
(5) Makovitzki, A.; Avrahami, D.; Shai, Y. *Proc. Natl. Acad. Sci. U. S. A.* **2006**, *103*, 15997.
(6) Wiedman, G.; Kim, S. Y.; Zapata-Mercado, E.; Wimley, W. C.; Hristova, K. *J. Am. Chem. Soc.* **2017**, *139*, 937.
(7) Krauson, A. J.; Hall, O. M.; Fuselier, T.; Starr, C. G.; Kauffman, W. B.; Wimley, W. C. *J. Am. Chem. Soc.* **2015**, *137*, 16144.
(8) Rathinakumar, R.; Wimley, W. C. *J. Am. Chem. Soc.* **2008**, *130*, 9849.
(9) Ong, Z. Y.; Wiradharma, N.; Yang, Y. Y. *Adv. Drug Delivery Rev.* **2014**, *78*, 28.
(10) O'Shea, E. K.; Klemm, J. D.; Kim, P. S.; Alber, T. *Science* **1991**, *254*, 539.
(11) Wolf, E.; Kim, P. S.; Berger, B. *Protein Sci.* **1997**, *6*, 1179.
(12) Presnell, S. R.; Cohen, F. E. *Proc. Natl. Acad. Sci. U. S. A.* **1989**, *86*, 6592.
(13) Peraro, M. D.; van der Goot, F. G. *Nat. Rev. Microbiol.* **2016**, *14*, 77.
(14) MacKinnon, R.; Cohen, S. L.; Kuo, A.; Lee, A.; Chait, B. T. *Science* **1998**, *280*, 106.
(15) Payandeh, J.; Scheuer, T.; Zheng, N.; Catterall, W. A. *Nature* **2011**, *475*, 353.
(16) Eshaghi, S.; Niegowski, D.; Kohl, A.; Molina, D. M.; Lesley, S. A.; Nordlund, P. *Science* **2006**, *313*, 354.
(17) Lunin, V. V.; Dobrovetsky, E.; Khutoreskaya, G.; Zhang, R.; Joachimiak, A.; Doyle, D. A.; Bochkarev, A.; Maguire, M. E.; Edwards, A. M.; Koth, C. M. *Nature* **2006**, *440*, 833.
(18) Hibbs, R. E.; Gouaux, E. *Nature* **2011**, *474*, 54.
(19) Hou, X.; Pedi, L.; Diver, M. M.; Long, S. B. *Science* **2012**, *338*, 1308.
(20) Lau, S. Y.; Taneja, A. K.; Hodges, R. S. *J. Biol. Chem.* **1984**, *259*, 13253.
(21) Mutter, M.; Vuilleumier, S. *Angew. Chem., Int. Ed. Engl.* **1989**, *28*, 535.
(22) Sasaki, T.; Kaiser, E. T. *J. Am. Chem. Soc.* **1989**, *111*, 380.
(23) Hill, C. P.; Anderson, D. H.; Wesson, L.; DeGrado, W. F.; Eisenberg, D. *Science* **1990**, *249*, 543.
(24) Schafmeister, C. E.; Miercke, L. J.; Stroud, R. M. *Science* **1993**, *262*, 734.
(25) Lovejoy, B.; Choe, S.; Cascio, D.; McRorie, D. K.; DeGrado, W. F.; Eisenberg, D. *Science* **1993**, *259*, 1288.
(26) Bryson, J. W.; Betz, S. F.; Lu, H. S.; Suich, D. J.; Zhou, H. X.; O'Neil, K. T.; DeGrado, W. F. *Science* **1995**, *270*, 935.
(27) Schafmeister, C. E.; LaPorte, S. L.; Miercke, L. J. W.; Stroud, R. M. *Nat. Struct. Biol.* **1997**, *4*, 1039.
(28) Gradišar, H.; Božič, S.; Doles, T.; Vengust, D.; Hafner-Bratkovič, I.; Mertelj, A.; Webb, B.; Šali, A.; Klavžar, S.; Jerala, R. *Nat. Chem. Biol.* **2013**, *9*, 362.
(29) Fletcher, J. M.; Harniman, R. L.; Barnes, F. R. H.; Boyle, A. L.; Collins, A.; Mantell, J.; Sharp, T. H.; Antognozzi, M.; Booth, P. J.; Linden, N.; Miles, M. J.; Sessions, R. B.; Verkade, P.; Woolfson, D. N. *Science* **2013**, *340*, 595.
(30) Wen, A. M.; Steinmetz, N. F. *Chem. Soc. Rev.* **2016**, *45*, 4074.
(31) Obana, M.; Silverman, B. R.; Tirrell, D. A. *J. Am. Chem. Soc.* **2017**, *139*, 14251.
(32) Tavenor, N. A.; Murnin, M. J.; Horne, W. S. *J. Am. Chem. Soc.* **2017**, *139*, 2212.
(33) Ren, C. L.; Shen, J.; Chen, F.; Zeng, H. Q. *Angew. Chem., Int. Ed.* **2017**, *56*, 3847.
(34) Ren, C. L.; Ng, G. H. B.; Wu, H.; Chan, K.-H.; Shen, J.; Teh, C.; Ying, J. Y.; Zeng, H. Q. *Chem. Mater.* **2016**, *28*, 4001.
(35) Ren, C. L.; Chen, F.; Zhou, F.; Shen, J.; Su, H. B.; Zeng, H. Q. *Langmuir* **2016**, *32*, 13510.
(36) Vargas Jentzsch, A.; Matile, S. *J. Am. Chem. Soc.* **2013**, *135*, 5302.
(37) Guo, Y.; Pogodin, S.; Baulin, V. A. *J. Chem. Phys.* **2014**, *140*, 174903.
(38) Shinde, S. V.; Talukdar, P. *Angew. Chem., Int. Ed.* **2017**, *56*, 4238.
(39) Nguyen, L. T.; Haney, E. F.; Vogel, H. J. *Trends Biotechnol.* **2011**, *29*, 464.
(40) Sani, M.-A.; Separovic, F. *Acc. Chem. Res.* **2016**, *49*, 1130.
(41) Ros, U.; García-Sáez, A. J. *J. Membr. Biol.* **2015**, *248*, 545.
(42) Rojko, N.; Anderluh, G. *Acc. Chem. Res.* **2015**, *48*, 3073.
(43) Gilbert, R. J. *Biochim. Biophys. Acta, Biomembr.* **2016**, *1858*, 487.
(44) Jo, S.; Kim, T.; Iyer, V. G.; Im, W. *J. Comput. Chem.* **2008**, *29*, 1859.
(45) Sun, H. *J. Phys. Chem. B* **1998**, *102*, 7338−7364.
(46) Wu, E. L.; Cheng, X.; Jo, S.; Rui, H.; Song, K. C.; Davila-Contreras, E. M.; Qi, Y.; Lee, J.; Monje-Galvan, V.; Venable, R. M.; Klauda, J. B.; Im, W. *J. Comput. Chem.* **2014**, *35*, 1997.
(47) Jo, S.; Lim, J. B.; Klauda, J. B.; Im, W. *Biophys. J.* **2009**, *97*, 50.
(48) Vanommeslaeghe, K.; Hatcher, E.; Acharya, C.; Kundu, S.; Zhong, S.; Shim, J.; Darian, E.; Guvench, O.; Lopes, P.; Vorobyov, I.; MacKerell, A. D. *J. Comput. Chem.* **2010**, *31*, 671.
(49) Jorgensen, W. L.; Chandrasekhar, J.; Madura, J. D.; Impey, R. W.; Klein, M. L. *J. Chem. Phys.* **1983**, *79*, 926.
(50) Essmann, U.; Perera, L.; Berkowitz, M. L.; Darden, T.; Lee, H.; Pedersen, L. G. *J. Chem. Phys.* **1995**, *103*, 8577.
(51) Martyna, G. J.; Tobias, D. J.; Klein, M. L. *J. Chem. Phys.* **1994**, *101*, 4177.
(52) Sidorov, V.; Kotch, F. W.; Abdrakhmanova, G.; Mizani, R.; Fettinger, J. C.; Davis, J. T. *J. Am. Chem. Soc.* **2002**, *124*, 2267.
(53) Schlesinger, P. H.; Ferdani, R.; Liu, J.; Pajewska, J.; Pajewski, R.; Saito, M.; Shabany, H.; Gokel, G. W. *J. Am. Chem. Soc.* **2002**, *124*, 1848.
(54) Gorteau, V.; Bollot, G.; Mareda, J.; Perez-Velasco, A.; Matile, S. *J. Am. Chem. Soc.* **2006**, *128*, 14788.
(55) Gorteau, V.; Bollot, G.; Mareda, J.; Matile, S. *Org. Biomol. Chem.* **2007**, *5*, 3000.
(56) Li, X.; Shen, B.; Yao, X.-Q.; Yang, D. *J. Am. Chem. Soc.* **2009**, *131*, 13676.
(57) Yamnitz, C. R.; Negin, S.; Carasel, I. A.; Winter, R. K.; Gokel, G. W. *Chem. Commun.* **2010**, *46*, 2838.
(58) Saha, T.; Dasari, S.; Tewari, D.; Prathap, A.; Sureshan, K. M.; Bera, A. K.; Mukherjee, A.; Talukdar, P. *J. Am. Chem. Soc.* **2014**, *136*, 14128.
(59) Saha, T.; Gautam, A.; Mukherjee, A.; Lahiri, M.; Talukdar, P. *J. Am. Chem. Soc.* **2016**, *138*, 16443.

DOI: 10.1021/jacs.8b04657
J. Am. Chem. Soc. 2018, 140, 8817−8826

(60) Wei, X.; Zhang, G.; Shen, Y.; Zhong, Y.; Liu, R.; Yang, N.; Almkhaizim, F. Y.; Kline, M. A.; He, L.; Li, M.; Lu, Z.-L.; Shao, Z.; Gong, B. *J. Am. Chem. Soc.* **2016**, *138*, 2749.
(61) Behera, H.; Madhavan, N. *J. Am. Chem. Soc.* **2017**, *139*, 12919.
(62) Ren, C. L.; Ding, X.; Roy, A.; Shen, J.; Zhou, S. Y.; Chen, F.; Yau Li, S. F.; Ren, H. S.; Yang, Y. Y.; Zeng, H. Q. *Chem. Sci.* **2018**, *9*, 4044.
(63) Izzo, I.; Licen, S.; Maulucci, N.; Autore, G.; Marzocco, S.; Tecilla, P.; De Riccardis, F. *Chem. Commun.* **2008**, 2986.
(64) Madhavan, N.; Robert, E. C.; Gin, M. S. *Angew. Chem., Int. Ed.* **2005**, *44*, 7584.
(65) Benke, B. P.; Aich, P.; Kim, Y.; Kim, K. L.; Rohman, M. R.; Hong, S.; Hwang, I.-C.; Lee, E. H.; Roh, J. H.; Kim, K. *J. Am. Chem. Soc.* **2017**, *139*, 7432.

DOI: 10.1021/jacs.8b04657
J. Am. Chem. Soc. 2018, 140, 8817−8826